Pressure-induced phase transitions and metallization in VO_2

Ligang Bai,[1,*] Quan Li,[2] Serena A. Corr,[3] Yue Meng,[1] Changyong Park,[1] Stanislav V. Sinogeikin,[1] Changhyun Ko,[4] Junqiao Wu,[4] and Guoyin Shen[1,†]

[1] *High Pressure Collaborative Access Team (HPCAT), Geophysical Laboratory, Carnegie Institute of Washington, Argonne, IL 60439, USA*
[2] *College of Materials Science and Engineering and State Key Laboratory of Superhard Materials, Jilin University, Chang Chun 130012, China*
[3] *School of Chemistry, University of Glasgow, Glasgow, United Kingdom*
[4] *Department of Materiasl Science and Engineering, University of California at Berkeley, Berkeley, California 94720, USA*

(Dated: March 19, 2015)

We report the results of pressure-induced phase transitions and metallization in VO_2 based on synchrotron x-ray diffraction, electrical resistivity, and Raman spectroscopy. Our isothermal compression experiments at room temperature and 383 K show that the room temperature monoclinic phase (M1, $P2_1/c$) and the high temperature rutile phase (R, $P4_2/mnm$) of VO_2 undergo phase transitions to a distorted M1 monoclinic phase (M1′, $P2_1/c$) above 13.0 GPa and to an orthorhombic phase ($CaCl_2$-like, $Pnnm$) above 13.7 GPa, respectively. Upon further compression, both high-pressure phases transform into a new phase (phase X) above 34.3 and 38.3 GPa at room temperature and 383 K, respectively. The room temperature M1-M1′ phase transition structurally resembles the R-$CaCl_2$ phase transition at 383 K, suggesting a second-order displacive type of transition. Contrary to previous studies, our electrical resistivity results, Raman measurements, as well as ab initio calculations indicate that the new phase X, rather than the M1′ phase, is responsible for the metallization under pressure. The metallization mechanism is discussed based on the proposed crystal structure.

PACS numbers: 82.35.Jk,71.30.+h,81.40.Vw,61.05.fm

I. INTRODUCTION

Transition metal oxides exhibit diverse polymorphism and interesting properties such as metal-insulator transitions (MIT),[1] high-temperature superconductivity,[2] and colossal magnetoresistance[3] largely because of the interplay of electronic and lattice degrees of freedom. Significant attention has been given to MIT, which may be triggered by temperature, electric field, pressure, chemical doping, ultrafast laser excitation, and ionizing radiation.[4–9] As was first observed by Morin,[10] VO_2 undergoes a first order transition at a modest temperature of 340 K from a high temperature paramagnetic metallic rutile (R) phase to a low temperature nonmagnetic insulating monoclinic (M1) phase. In the R-phase (space group $P4_2/mnm$), V ions, nominally V^{4+} in $3d^1$ configuration, are equally spaced along the c-axis and located at the center of oxygen octahedra. According to a crystal-field model proposed by Goodenough,[11] the 3d orbitals are split into t_{2g} and empty e_g^σ orbitals, with t_{2g} further split into an e_g^π doublet and an a_{1g} singlet. The a_{1g} orbital with V-V pair bonding is directed along the c axis, and the overlap of a_{1g} and e_g^π orbitals in the rutile structure is considered to be responsible for its metallic character. In the M1 phase (space group $P2_1/c$), V ions are dimerized and tilted with respect to the c-axis, which elevates the e_g^π band and splits a_{1g} into bonding and antibonding orbitals, leading to an insulating state. This simple picture is helpful for understanding and interpreting the MIT. However, density functional theory (DFT) calculations did not predict the correct band gap for the M1 phase using the experimental structural data in the absence of strong electron correlations,[12,13] suggesting essential roles of electron correlation. Recently, after considering full relaxation of the volume and the atomic structure, the insulating state of the M1-phase was predicted by DFT without strong electron correlation.[14] In other words, the MIT in VO_2 may be dominantly driven by lattice (or Peierls distortion).[15,16] From experiments, several researchers claimed that electron-electron correlations cannot be ignored.[17] More recent studies demonstrated that the structural and electronic transitions can be decoupled by temperature,[18] pressure,[19] and ultrafast laser excitation.[20] It has been also pointed out that the possibility of the MIT may be viewed as a consequence of crystalline distortion rather than a cause of it.[21–23] Despite extensive experimental and theoretical studies, the mechanism of the MIT is still under debate: whether the structural phase transition (Peierls distortion) is the major cause for the temperature driven MIT, or if strong electron correlations (Mott effect) are responsible for opening the band gap of the low-temperature phase.

The application of external pressure provides a unique way to investigate the relationship between structural and electronic properties. It also provides a possible route to decouple the electronic and structural phase transitions. For example, the degree of electron correlation may be changed by tuning the band width under external pressure. Several previous high-pressure studies have been carried out for VO_2. The resistiv-

ity measurements showed that the transition temperature of the MIT increases linearly up to 4 GPa.[22,24] Recent studies using Raman and infrared spectroscopy techniques showed a phase transition from M1 phase to an isostructural phase exhibiting enhanced metallicity above 12 GPa.[19,25,26] An x-ray diffraction (XRD) study under high pressure showed changes in lattice compression of the $b-c$ plane of the M1 phase, which was considered as an evidence for the enhanced metallicity.[27] Because of the isostructural nature of the transition, the authors proposed that the pressure-enhanced metallicity in VO_2 is mainly driven by suppressing electron-electron correlation, rather than of the Peierls distortion. However, their data only provided evidence of metallization process, but lacked direct evidence for a room temperature metallic phase within a monoclinic structure.[19] It is also unclear the role of structural changes (Peierls distortion) in the MIT, and whether the electron correlation alone, tuned by pressure, can induce the MIT. To address these questions, we have studied the pressure effect on structures and electrical resistivity of VO_2 up to 55.3 and 61.4 GPa, respectively. We identify that the isostructural phase transition at 13 GPa is a second-order type and is not responsible for metallization. Upon further compression, a high pressure phase X with monoclinic structure was observed. The Raman and resistivity results indicate that the metallization is achieved in the phase X. Its crystal structure is discussed to explain the metallization mechanism.

II. EXPERIMENTAL PROCEDURES

A. Sample preparation

Pure single phase VO_2 powder samples were used for all the measurements except for the Raman measurements where a single crystal sample was used. The powder samples were prepared in vacuum sealed silica ampoules using a stoichiometric mixture of V_2O_5 (99.9%, Alfa Aesar) and V_2O_3, with the latter obtained by reduction of V_2O_5 in 5% H_2/N_2 gas at 900C.[7] All experiments were performed in diamond-anvil cells (DAC) with anvils of 300 μm culet size and rhenium as gasket material.

B. X-ray diffraction

High-pressure powder XRD measurements were carried out at 16-ID-B and 16-BM-D beamlines of the High Pressure Collaborative Access Team (HPCAT) facility, at the Advanced Photon Source (APS), Argonne National Laboratory (ANL). Two separate isothermal experiments were performed at room temperature and at 383 K up to 55.3 and 53.0 GPa, respectively. Neon was used as pressure-transmitting medium, loaded by using a high-pressure gas-loading system.[28] Pressure was determined by the ruby-fluorescence method.[29] The x-ray beam wavelength was 0.3979 Å. Diffraction patterns were recorded using a MAR3450 imaging plate detector. The intensity versus 2θ patterns were obtained using the FIT2D software.[30] Le Bail whole-profile refinements of the XRD patterns were performed using the FULLPROF software package.[31] Equation of state analysis was performed by means of EOSFIT software.[32]

C. Raman spectroscopy

We used the micro-Raman spectrometer at GSECARS sector 13 for Raman measurements. The system is equipped with an argon-ion laser (=514.5 nm, 50 mW) and a focused spot of diameter 4 m at the sample position. A Spec-0.5m spectrograph was used together with an 1800 grooves/mm grating and a liquid nitrogen cooled CCD detector. Neon was used as pressure-transmitting medium. Similarly, pressure was measured using the ruby fluorescence technique.[29]

D. Resistivity measurements

High-pressure electrical resistivity measurements were performed using the standard four-probe technique in a diamond anvil cell up to 61.4 GPa. Rhenium metal gasket was insulated with a mixture of the epoxy and cubic boron nitride. Four platinum leads were arranged to contact the sample in the chamber. The pressure medium for resistivity measurement is NaCl powder. The resistance was determined by the Van de Pauw method.[33] Pressure was measured using the ruby fluorescence technique.[29]

III. AB INITIO CALCULATIONS

We performed DFT calculations with Vienna Ab-initio Simulation Package (VASP) code.[34] The calculations employed the projector augmented wave (PAW) method and the generalized gradient approximation (PBE-GGA) for electron exchange-correlation interaction.[35] An energy cutoff of 800 eV for the plane-wave expansion and Monkhorst-Pack k-point meshes of 10×10×10 and 7×7×7 for the rutile and monoclinic structures in the Brillouin zone respectively, produced enthalpy results well converged to below 1 meV/fu. We had performed systematical tests to evaluate the U values for the GGA+U calculations. All internal atomic coordinates were relaxed until the calculated forces were less than 0.005 eV/Å, and the deviation of the stress tensor from the diagonal hydrostatic form was less than 0.1 GPa. The calculations for the density of states were carried out after the full relaxation of the volume and atomic positions under pressures.

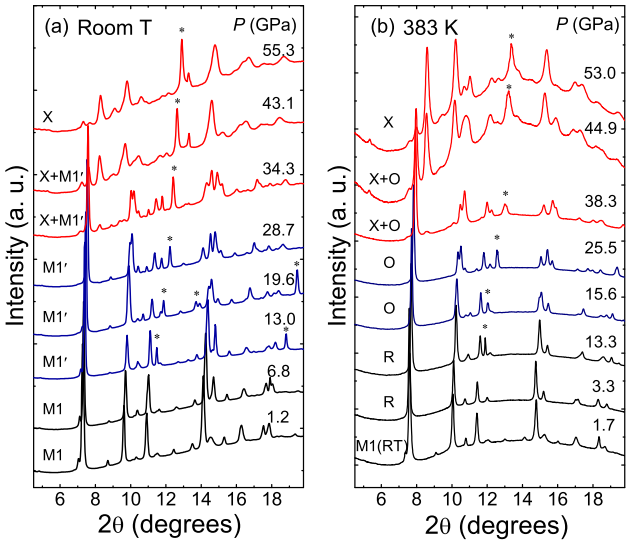

FIG. 1. (color online)High-pressure x-ray diffraction patterns of VO_2 collected at (a) room temperature and (b) 383 K, where R and O denote rutile and $CaCl_2$ phases. The pattern at 1.7 GPa in (b) is collected at room temperature for comparison. Stars indicate diffraction peaks from Ne pressure medium.

IV. RESULTS

A. Pressure-induced structural changes from x-ray diffraction

Typical angle dispersive powder x-ray diffraction data for VO_2 at pressures up to 55.3 GPa at room temperature are shown in Fig. 1(a). All the observed diffraction reflections obtained at 1.2 GPa can be indexed with a M1 monoclinic structure. The overall M1 structure remains unchanged up to 13.0 GPa, above which some of the diffraction peaks start to broaden or split. Despite these changes, the diffraction patterns can still be well indexed with a monoclinic symmetry up to 28.7 GPa with a distorted M1 structure of the same space group ($P2_1/c$), which is in general agreement with a previous diffraction study.[27] We refer the distorted phase as M1′ because of its similarity to the M1 phase.

As pressure was further increased to 34.3 GPa, new diffraction peaks appear in regions of 2θ between 6° and 9° (Fig. 1(a)). At 43.1 GPa, the intensity of the peaks from M1′ phase decreases considerably and the new diffraction peaks become dominant at 55.3 GPa. The changes in diffraction peaks clearly indicate a new phase (called phase X) starting at 34.3 GPa and both phases (M1′, X) coexist over a wide pressure range of more than 10 GPa.

Figure 1(b) shows the evolution of x-ray diffraction patterns at elevated temperature of 383 K with increasing pressure. The first pattern collected at room temperature is the pure M1 phase. After heating to 383 K at a pressure of 3.3 GPa, the M1 phase transforms to the rutile phase. Above 13.3 GPa, an orthorhombic distortion is obvious from the splitting of (hkl) diffraction lines where hk. This is consistent with the structural distortion from rutile to $CaCl_2$ crystal structures observed in other rutile-type oxides such as CrO_2,[36] MnO_2,[37] RuO_2,[38] SiO_2.[39] The phase transition from rutile to $CaCl_2$ is a strain-driven, second-order distortive type and proceeds via a rotation of the distorted VO_6 octahedra about the c-axis. The $CaCl_2$ phase is stable up to 38.3 GPa, above which the diffraction peaks from the phase X appear, similar to those at room temperature. At 53.0 GPa, the phase X becomes the dominant phase.

B. Pressure dependence of the unit cell parameters and the equations of state

The variations of the unit cell parameters of VO_2 with increasing pressure at room temperature and 383K were obtained by Le Bail whole-profile fitting to each diffraction patterns. Figure 2(a) shows the evolution of the monoclinic lattice parameters as a function of pressure at room temperature, where we compare it with the results of a previous study[27] and our theoretical values calculated within the GGA+U (U=1, 2, 3, and 4). The isostructural phase transition M1-M1′ at 13 GPa is accompanied by an anomalous compression behavior of the b and c lattice parameters, while the a lattice parameter apparently does not exhibit clear unusual behavior. This is in agreement with previous studies.[27]

From theoretical calculations as shown in Fig. 2(a), we find that the effect of U on the compression behavior is relatively large on the $b-c$ plane compared to that of a-axis. The overall compression behavior at a given U is almost parallel to the trends of experimental data. Therefore, U may be not sensitive to pressure.

The structure of the M1 phase can be related to that of the high-temperature rutile phase by lattice parameter relations ($\boldsymbol{a}^R_{M1}$=2$\boldsymbol{c}_R$, $\boldsymbol{b}^R_{M1}$=$\boldsymbol{a}_R$, $\boldsymbol{c}^R_{M1}$=$\boldsymbol{a}_R$-$\boldsymbol{c}_R$). This notation is used to show the compression of the lattice parameters of the rutile and $CaCl_2$ phases (Fig. 2(b)) for comparison purpose. Its interesting to note that the R-$CaCl_2$ transition pressure coincides with that of the M1-M1′ transition. It can also be seen that the compression behaviors of M1 and M1′ phases are similar to those of R and $CaCl_2$ phases, indicating that the distortion from M1 to M1′ phase at ambient temperature is analogous to the transition of rutile to $CaCl_2$ phase at high temperature.

The pressure vs volume data at room temperature and 383 K are plotted in Fig. 3(a) and (b) respectively. Equations of states (EOS) are determined by fitting the compression data using the third-order Birch-Murnaghan equation.

$$P = \frac{3B_0}{2}\left[\left(\frac{V_0}{V}\right)^{7/3} - \left(\frac{V_0}{V}\right)^{5/3}\right] \times$$

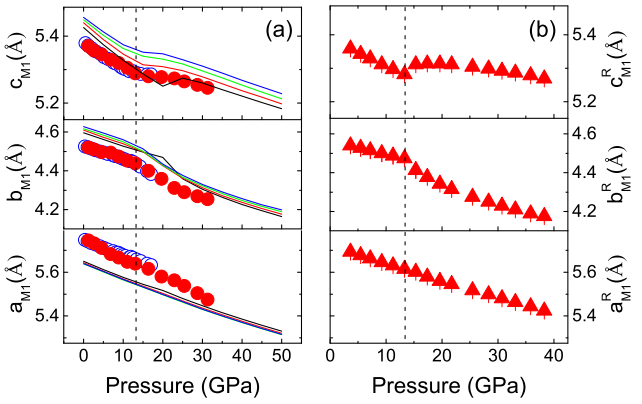

FIG. 2. (color online)Pressure dependence of a, b, and c unit cell parameters of the monoclinic structure. Solid red circles are x-ray diffraction data from this study, solid lines are results from ab initio GGA+U (U=1 black, 2 red, 3 green, 4 blue; J=0.68) calculations in this study. Open circles are from ref [27] ; (b) Pressure dependence of unit cell parameters of the rutile and $CaCl_2$ structures. To compare with the compression behavior of monoclinic phases, equivalent lattice parameters ($\boldsymbol{a}^R_{M1}$=2$\boldsymbol{c}_R$, $\boldsymbol{b}^R_{M1}$=$\boldsymbol{a}_R$, $\boldsymbol{c}^R_{M1}$=$\boldsymbol{a}_R$-$\boldsymbol{c}_R$) are used.

TABLE I. Comparison of the EOS parameters for different phases in VO_2

phase	V_0(Å^3)	B_0(GPa)	Reference
M1	118.32(4)	213(2)	This study
M1	117.98(4)	142(1)	Ref. 27
M1	118.01(1)	207(3)	Refit Ref. 27
M1′	120.20(30)	167(4)	This study
Rutile	59.75(2)	190(2)	This study
$CaCl_2$	60.13(6)	171(2)	This study

$$\left\{1+\frac{3}{4}(B_0'-4)\left[\left(\frac{V_0}{V}\right)^{2/3}-1\right]\right\} \qquad (1)$$

where P, V, and V_0 denote pressure, volume at pressure P, and volume at ambient pressure, respectively. B_0 and B_0' are the zero-pressure bulk modulus and its pressure derivate. The B_0' is fixed to 4 for comparison.As shown in the Table I, at room temperature for the M1 phase the bulk modulus 213(2) GPa is higher than that 167(4) GPa for the M1′ phase, at 383 K where 190(2) GPa for rutile phase is higher than 171(2) GPa for the $CaCl_2$ phase. This is normal for strain-driven distortive-type transition at high pressures. Our data on compression is consistent with the reported data[27] (Fig. 3(a)). However the resultant bulk modulus is larger than their value[27], thereby we refit the P-V data of Ref. 27, yielding a bulk modulus that are very close to ours.

C. Pressure dependence of Raman spectra

There are nine Ag and nine Bg Raman active modes in M1 phase of VO_2 (space group $P2_1/c$). The measured

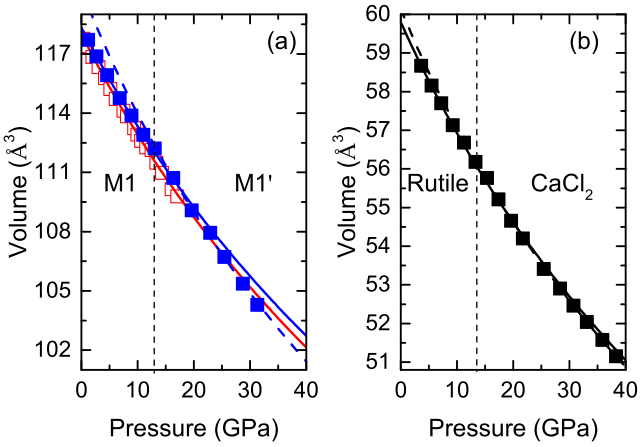

FIG. 3. (color online)Pressure versus volume data for VO_2 at (a) room temperature and (b) 383 K, dashed vertical lines denote transition pressures from (a) M1 to M1′ phases and (b) rutile to $CaCl_2$ phases. (a) Solid blue squares are data from present XRD, open red squares are previous data from Ref. 15. The solid and dash blue curves indicate our EOS for M1 and M1′ phases respectively, the solid red curves indicate the refitting EOS using data from Ref. 15. (b) Solid black squares are data from present XRD, the solid and dash curves indicate our EOS for rutile and $CaCl_2$ phases respectively.

Raman spectra at high pressures and room temperature are shown in Fig. 4. Ten modes marked as A-J can be identified. With increasing pressure up to 27.8 GPa, all of the Raman peaks shift to higher frequencies. The peak C is broadened and finally splits above 27.8 GPa. It is noted that all the Raman peaks become much weaker above 38.7 GPa and finally disappear above 42.2 GPa. Generally speaking, vanishing of Raman peak can be accounted for in two ways: (1) a structural transition where no Raman mode is allowed by symmetry, (2) a transition to a metallic state where the Raman signal becomes extremely weak due to limited penetration depth of exciting laser. In this case, our XRD results clearly show that the structure in this pressure range cannot be cubic (see below). So the disappearance of the Raman signal under pressure can be taken as a supporting evidence of metallization.

The pressure dependence of the Raman peaks is plotted in Fig. 5, which can be classified into two regions: 100-350 cm^{-1} (region 1, Fig. 5(a)) and 350-800 cm^{-1} (region 2, Fig. 5(b)). All the Raman frequencies in the region 2 increase smoothly with pressure and can be fitted to a quadratic function of pressure, whereas the Raman frequencies in region 1 display more distinctive features. As shown in Fig. 5(a), the pressure dependences of the Raman shifts can be divided into three sub-regions indicated by the vertical dashed lines. Below 12.4 GPa, all modes in the region 1 (except mode A) shift slightly to higher frequencies with increasing pressure. The lowest mode A shifts to high frequency with pressure faster than other modes, and displays a slight slope change at 12.4

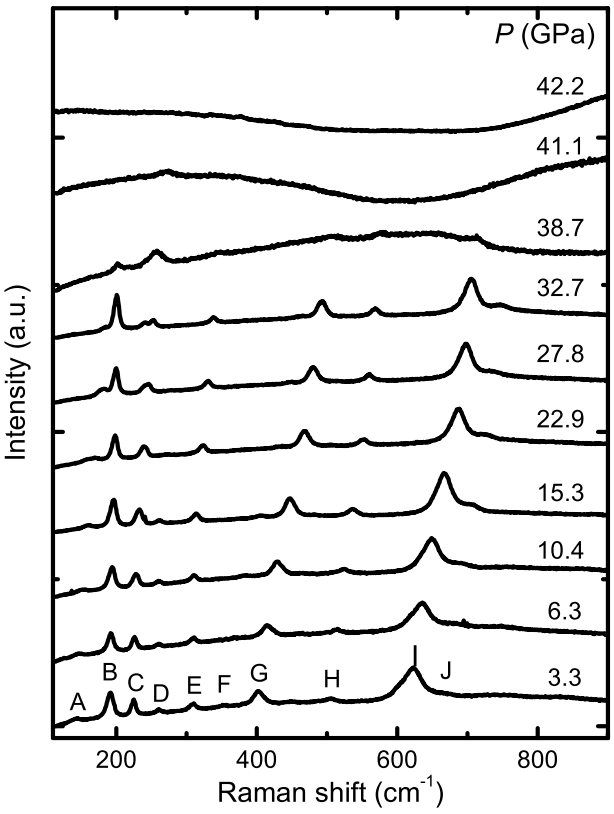

FIG. 4. Raman spectra of VO_2 measured at high pressures and ambient temperature. The phonon peaks are labeled by letters from A to J.

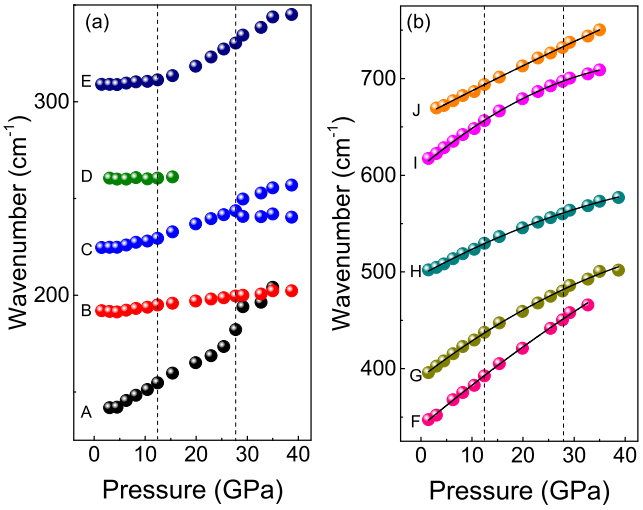

FIG. 5. (color online): Pressure dependencies of phonon frequencies of VO_2 at ambient temperature. Phonon modes from A to J corresponding to those in Fig. 4. (a) phonon modes between 100 and 350 cm^{-1}, and (b) phonon modes between 350 and 800 cm^{-1}. Changes in Raman peaks are indicated by the vertical dash lines.

GPa and a jump at 27.8 GPa. Above 12.4 GPa, the B, C and E modes show rather sharp changes in slope. These observations are in general agreement with the trends reported previously below 19.1 GPa.[19] The slope changes of the B, C and E modes at 12.4 GPa are related to the phase transition M1-M1′. Further increasing pressure to above 27.8 GPa leads to the splitting of mode C and discontinuities in the pressure dependencies of other modes, which is related to the appearance of the phase X as observed in XRD.

D. Electrical resistivity under pressure

Figure 6 presents the electrical resistivity up to 61.4 GPa, determined by using the equation $\rho=(\pi tR/\ln 2)$, where R is the resistance, and t is the thickness of the sample.[40] The sample thickness is estimated from the equation of state for VO_2 (Table I). The resistivity is 0.02 Ωm at 5.3 GPa, in the range of reported values of M1 phase.[21] We find a dramatic reduction in resistivity with increasing pressure by more than five orders of magnitude, from 10^{-2} Ωm (at 5.3 GPa) to 10^{-6} Ωm (at 61.4 GPa). A noticeable change in slope was observed at pressure of 14 GPa which is related to the phase transition from M1 to M1′ at room temperature as observed in our x-ray diffraction and Raman experiments. The resistivity nonlinearly drops with increasing pressure above 23.3 GPa, indicating the start of the phase transition from M1′ to X. With the pressure increased to greater than 37.7 GPa, the electrical resistivity levels off, and saturates at the level of approximately ∼4-5×10^{-6} Ωm, which is comparable to that of metallic rutile VO_2 (from 2.3×10^{-6} Ωm at 333 K to 5.0×10^{-6} Ωm at 800 K).[41] The slightly lower transition pressure from M1′ to phase X compared to XRD and Raman results may be due to the different pressure-transmitting media used in our experiments.

E. Electronic properties from ab initio calculations

The dependence of the band gap on electron correlation U for the M1 phase of VO_2 is shown in Fig, 7(a). It can be seen that there is an open band gap of 0.13 eV at U=0 after full relaxation of atomic positions and lattice parameters. The band gap increases with U almost linearly. The experimental measured band gap (∼0.6 eV) for the M1 phase[42] corresponds to an U value of 3.3 eV, which is not sensitive to pressurization from the results of our structural studies. Fig. 7(b) illustrates the two different behaviors of band gap change with pressure in the pressure range from 0 to 40 GPa. We observed a clear change on the slope at the M1 to M1′ phase transition, however we did not get the closing of the band gap in either M1 or M1′ phases under pressure.

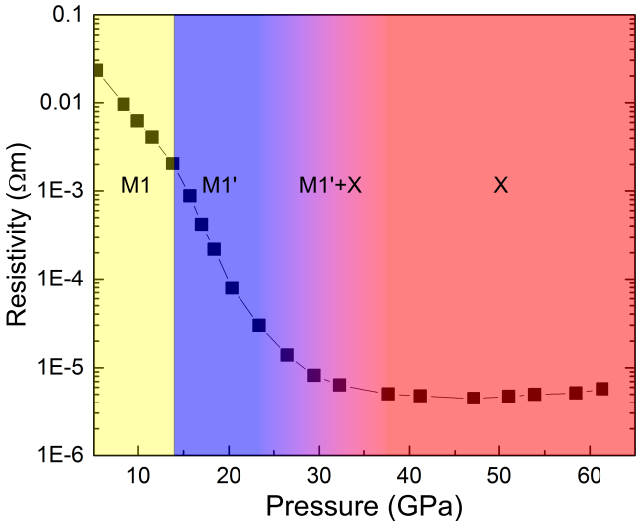

FIG. 6. (color online)Pressure dependence of electrical resistivity of VO_2 at ambient temperature. The transition pressures are indicated by the vertical lines.

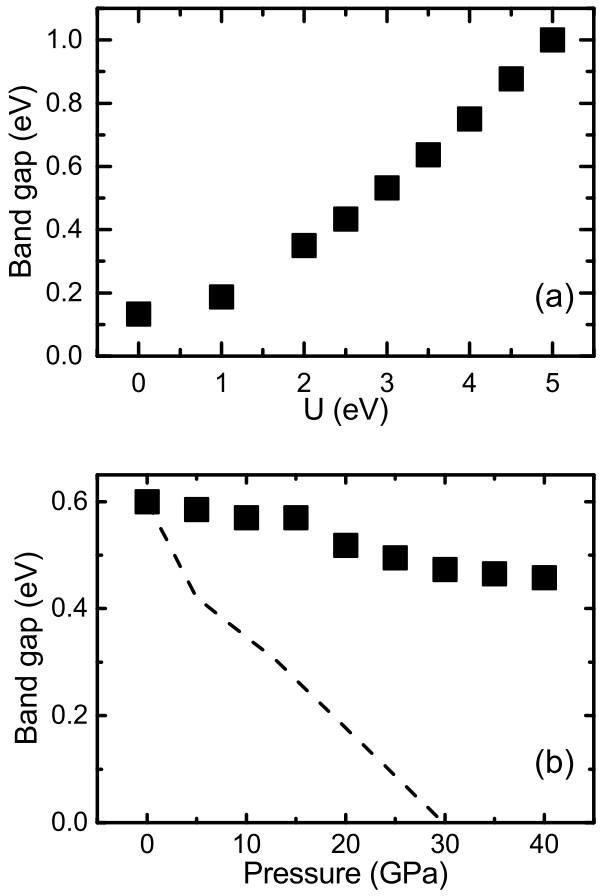

FIG. 7. (a) Band gap E_g as a function of Hubbard parameter U. (b) The band gap as a function of pressure (solid square: calculations, dash line: deduced from resistivity).

V. DISCUSSIONS

The M1-M1′ phase transition at 13 GPa is associated with anisotropic compression along crystallographic directions, and can be considered as isostructural transition. This conclusion is consistent with those in previous XRD studies.[27] From comparison with high temperature phase transition rutile-$CaCl_2$, The M1′ structure can be viewed as a monoclinic structure of $CaCl_2$-type and the phase transition M1-M1′ is likely of second order, so the volume change and atomic displacements at the transition pressure are subtle and continuous. This second order transition suggests that the rearrangement of V-V chains is unlikely across this transition. This is also supported by the theoretical simulation, which shows that the V-V dimers (Peierls distortion) still exist in the M1′ phase.

More importantly this phase transition was believed to be related to an optical gap filling metallization process by Arcangeletti *et al*. based on the mid-IR experiments.[19] As shown in Fig. 6, our resistivity results also show a fast decrease with increasing pressure below 30 GPa. The resistivity obeys Arrhenius law at all pressures: $\rho_0 = Aexp(E_g/2k_BT)$ and $\rho = Aexp(E'_g/2k_BT)$, where ρ_0 and ρ are the resistivities at ambient pressure and high pressure respectively, E_g and E'_g are the band gaps at ambient pressure and high pressure respectively, k_B is Boltzmann's constant, and T is temperature. Then at a constant temperature the band gap can be obtained by $ln(\rho - \rho_0) = (E_g - E'_g)/2k_BT$. As shown in Fig. 7(b), the band gap at room temperature derived by the above equation decreases much faster than that from ab initio calculations and closes at about 30 GPa, at which VO_2 is still in the M1′ phase pressure according our XRD and Raman measurements. If the resistivity measurement could reflect the band gap very well, the metallization would occur in the M1′ phase under pressure, which would overall agree with previous IR measurements.[19] However, as pointed by Berglund and Guggenheim,[21,22] the VO_2 samples contain donor- and/or acceptor-like states within the energy gap. Hence, the reduction of activation energy from resistivity measurements and optical gap from mid-IR measurements are largely contributed from the existence of defects, and may not directly relate to band gap closure. Furthermore, our theoretical calculations show that correlation effect U is almost constant in the M1 and M1′ phase and the band gap is not sensitive under hydrostatic pressure. Therefore, pressure does not introduce metallization in the M1 and M1′ phases, i.e. pressure alone cannot decouple the electronic and the structural transition.

Our XRD results show that the phase transition from M1′ to X starts at 34.3 GPa, with two phases coexistence spanning over 10 GPa. The Raman and resistivity measurements show similar results. Such a wide coexistence pressure range indicates that this transition is kinetically hindered and first order. Both the disappearance of the Raman signal above 42.2 GPa and the level-off of the

resistivity above 37.7 GPa suggest that the phase X is metallic.

The structure of the high-pressure phase X of VO_2 at 53 GPa can be indexed with a monoclinic unit cell a=3.586 Å, b=9.686 Å, c= 5.207 Å, β=94.63°, V=179.73 Å^3, using DICVOL. We consider the transition from rutile to X phase in VO_2 analogous to those in TiO_2[43] and NbO_2[44] from rutile and distorted-rutile structures to baddeleyite and baddeleyite-related structures at 12.0 and 20.3 GPa, respectively. These transitions are accompanied by the coordination number increase from 6 to 7. In the phase X of VO_2, similar in NbO_2, the oxide anions may occupy a baddeleyite-like arrangement. If we assume Z=8 in phase X, the volume change at the transition between M1′/$CaCl_2$ phases and phase X is estimate to be 10%, this compares well with the ΔV in TiO_2 (11.3%) and NbO_2 (10.1%). So the phase X is most likely a baddeleyite-related structure, although the detail structure refinement is not possible due to the insufficient quality of the XRD patterns. Another evidence of this phase transition is from Raman measurements, since the lowest Raman modes in the rutile phase is related to the rotation of the MO_6 (M=metal ion) octahedral around the z axis. So the mode A can be assigned to the octahedral rotation mode. As shown in Fig. 5a, the mode A only shows a slight slope change in the first phase transition at 12 GPa, which indicates that MO_6 octahedron is stable from M1 to M1′ phases. Whereas a sharp change in the second phase transition at 27 GPa was observed, which suggests that the phase X is related to a strengthening of octahedron induced by coordination change.

The Raman modes B and C were associated with the paring and tilting motions of V-V dimers by mapping the monoclinic phase onto the tetragonal lattice configuration.[25] The splitting of the mode C above 27.8 GPa then should suggest an activation of the vibration from the new V-V bond in the phase X. Actually in the low pressure Rutile/M1 and $CaCl_2$/M1′ structures, one-dimensional V-V chains are through edge-sharing VO_6 octahedra along the c axis of the Rutile and $CaCl_2$ structures. In the baddeleyite-related structure phase X, each seven-coordinate polyhedral VO_7 are edge-sharing with four of them. The unique one-dimensional V-V chains no longer exist. The increasing in dimensionality will destroy Peierls distortion and rearrange the V-V bond which will introduce metallization in this high-pressure phase X.

VI. CONCLUSIONS

In summary, the structural, vibrational, and electronic properties of VO_2 have been investigated under pressure by a series of experiments and calculations. High-pressure x-ray diffraction measurements performed at room and high temperature show that the M1 phase first goes through a displacive distortion above 13.0 GPa at room temperature, which closely resembles the rutile-$CaCl_2$ phase transition above 13.7 GPa at high temperature. The distortion of M1 phase is well reproduced by our ab initio calculations. Furthermore, theoretical calculations indicate that there is no metallization in the M1 and M1′ phases where Peierls distortion exists. Upon further compression to 34.3/38.3 GPa, a new phase transition is observed at room or high temperature. The new phase-X can be indexed on a monoclinic unit cell of baddeleyite-like structure. The metallization can only be occurred in phase X based on our Raman and electrical resistivity measurements. Our experimental and theoretical results suggest that the pressure-induced MIT in VO_2 is driven by a structural transition. Further experimental and theoretical studies on the structure of the phase X are necessary to completely characterize the pressure-induced metallization process and to understand the pressure-induced MIT in VO_2.

ACKNOWLEDGMENTS

We thank Jianbo Zhang for resistivity measurement help. This research is supported by DOE No. DE-FG02-99ER45775 and DOE No. DE-NA0001974. This work was performed at HPCAT (Sector 16), Advanced Photon Source (APS), Argonne National Laboratory (ANL). HPCAT operations are supported by DOE-NNSA under Award No. DE-NA0001974 and DOE-BES under Award No. DE-FG02-99ER45775, with partial instrumentation funding by NSF. The work at Berkeley was supported by a NSF CAREER Award under Grant DMR-1055938. We thank GSECARS, at the APS, ANL for the use of their gas loading and Raman setup. Use of the Advanced Photo Source is supported by the DOE Office of Science, Office of Basic Energy Sciencs, under Contract No. DE-AC02-06CH11357.

* lbai@carnegiescience.edu
† gshen@carnegiescience.edu

[1] M. Imada, A. Fujimori, and Y. Tokura, Reviews of Modern Physics **70**, 1039 (1998).
[2] D. C. Johnston, Advances in Physics **59**, 803 (2010).
[3] D. N. Basov, R. D. Averitt, D. van der Marel, M. Dressel, and K. Haule, Reviews of Modern Physics **83**, 471 (2011).
[4] A. Asahara, H. Watanabe, H. Tokoro, S.-i. Ohkoshi, and T. Suemoto, Physical Review B **90**, 014303 (2014).
[5] A. Yamasaki, M. Feldbacher, Y.-F. Yang, O. K. Andersen, and K. Held, Physical Review Letters **96**, 166401 (2006).

[6] V. Ponnambalam, S. Parashar, A. R. Raju, and C. N. R. Rao, Applied Physics Letters **74**, 206 (1999).
[7] S. A. Corr, D. P. Shoemaker, B. C. Melot, and R. Seshadri, Physical Review Letters **105**, 056404 (2010).
[8] J. M. Valles, A. E. White, K. T. Short, R. C. Dynes, J. P. Garno, A. F. J. Levi, M. Anzlowar, and K. Baldwin, Physical Review B **39**, 11599 (1989).
[9] K. E. Smith and V. E. Henrich, Physical Review B **50**, 1382 (1994).
[10] F. Morin, Physical Review Letters **3**, 34 (1959).
[11] J. B. Goodenough, Journal of Solid State Chemistry **3**, 490 (1971).
[12] B.-C. Shih, T. A. Abtew, X. Yuan, W. Zhang, and P. Zhang, Physical Review B **86**, 165124 (2012).
[13] Z. Zhu and U. Schwingenschlögl, Physical Review B **86**, 075149 (2012).
[14] S. Kim, K. Kim, C.-J. Kang, and B. I. Min, Physical Review B **87**, 195106 (2013).
[15] R. M. Wentzcovitch, W. W. Schulz, and P. B. Allen, Physical Review Letters **72**, 3389 (1994).
[16] V. Eyert, Annalen der Physik **11**, 650 (2002).
[17] A. Zylbersztejn, Physical Review B **11**, 4383 (1975).
[18] J. Laverock, S. Kittiwatanakul, A. A. Zakharov, Y. R. Niu, B. Chen, S. A. Wolf, J. W. Lu, and K. E. Smith, Physical Review Letters **113**, 216402 (2014).
[19] E. Arcangeletti, L. Baldassarre, D. Di Castro, S. Lupi, L. Malavasi, C. Marini, A. Perucchi, and P. Postorino, Physical Review Letters **98**, 196406 (2007).
[20] W.-P. Hsieh, M. Trigo, D. A. Reis, G. Andrea Artioli, L. Malavasi, and W. L. Mao, Applied Physics Letters **104**, 021917 (2014).
[21] C. Berglund and H. Guggenheim, Physical Review **185**, 1022 (1969).
[22] C. Berglund and A. Jayaraman, Physical Review **185**, 1034 (1969).
[23] A. Cavalleri, T. Dekorsy, H. H. W. Chong, J. C. Kieffer, and R. W. Schoenlein, Physical Review B **70**, 161102 (2004).
[24] C. H. Neuman, A. W. Lawson, and R. F. Brown, The Journal of Chemical Physics **41**, 1591 (1964).
[25] C. Marini, E. Arcangeletti, D. Di Castro, L. Baldassare, A. Perucchi, S. Lupi, L. Malavasi, L. Boeri, E. Pomjakushina, K. Conder, and P. Postorino, Physical Review B **77**, 235111 (2008).
[26] C. Marini, L. Baldassarre, M. Baldini, A. Perucchi, D. Di Castro, L. Malavasi, S. Lupi, and P. Postorino, High Pressure Research **30**, 55 (2010).
[27] M. Mitrano, B. Maroni, C. Marini, M. Hanfland, B. Joseph, P. Postorino, and L. Malavasi, Physical Review B **85**, 184108 (2012).
[28] M. Rivers, V. B. Prakapenka, A. Kubo, C. Pullins, C. M. Holl, and S. D. Jacobsen, (2008).
[29] H. K. Mao, J. Xu, and P. M. Bell, Journal of Geophysical Research **91**, 4673 (1986).
[30] A. P. Hammersley, S. O. Svensson, M. Hanfland, A. N. Fitch, and D. Hausermann, High Pressure Research **14**, 235 (1996).
[31] J. Rodríguez-Carvajal, Physica B: Condensed Matter **192**, 55 (1993).
[32] R. J. Angel, Reviews in Mineralogy and Geochemistry **41**, 35 (2001).
[33] van der Pauw, Philips Research Reports **13**, 1 (1958).
[34] G. Kresse and J. Furthmuller, Physical Review B **54**, 11169 (1996).
[35] J. P. Perdew, K. Burke, and M. Ernzerhof, Physical Review Letters **77**, 3865 (1996).
[36] B. R. Maddox, C. S. Yoo, D. Kasinathan, W. E. Pickett, and R. T. Scalettar, Physical Review B **73**, 144111 (2006).
[37] J. Haines, J. Léger, and S. Hoyau, Journal of Physics and Chemistry of Solids **56**, 965 (1995).
[38] J. Haines and J. M. Léger, Physical Review B **48**, 13344 (1993).
[39] K. J. Kingma, R. E. Cohen, R. J. Hemley, and H.-k. Mao, Nature **374**, 243 (1995).
[40] X. Huang, C. Gao, Y. Han, M. Li, C. He, A. Hao, D. Zhang, C. Yu, G. Zou, and Y. Ma, Applied Physics Letters **90**, 242102 (2007).
[41] P. B. Allen, R. M. Wentzcovitch, W. W. Schulz, and P. C. Canfield, Phys. Rev. B **48**, 4359 (1993).
[42] H. Verleur, A. Barker, and C. Berglund, Physical Review **172**, 788 (1968).
[43] L. Gerward and J. Staun Olsen, Journal of Applied Crystallography **30**, 259 (1997).
[44] J. Haines, J. M. Léger, A. S. Pereira, D. Häusermann, and M. Hanfland, Physical Review B **59**, 13650 (1999).